Research Article

Nanostructured and surface functionalized corncob as unique adsorbents for anionic dye remediation

Ayoade L. Adejumo[1] · Luqmon Azeez[2] · Abdulrasaq O. Oyedeji[3] · Rasheed O. Adetoro[1] · Fatai A. Aderibigbe[4]

Abstract

This study describes synthesis and characterization of corncob (CC), corncob nanocellulose (CCNC) and functionalized corncob (FCC) as unique adsorbents for methyl orange (MO) removal. Nanocellulose was synthesized via H_2SO_4 hydrolysis and functionalization was achieved using H_3PO_4. All adsorbents were characterized by scanning electron microscopy coupled with energy dispersive X-ray and Fourier transform infra-red spectroscopy. Functionalization modified surface chemistry (disappearance of OH and appearance of PO_4^{3-}), increased percentage carbon by 41.42% and produced well-developed pores. Nanocellulose retained intrinsic chemical properties of corncob though more porous with enhanced surface functionality prompted by more intense functional groups peaks and appearance of SO_4^{2-}. Maximum adsorption of MO occurred at pH 3.01, 4.11 and 2.09 for CC (54.34%), FCC (77.1%) and CCNC (96.81%) respectively. Adsorption parameters were fitted to four adsorption isotherms with Langmuir being the most appropriate to describe the adsorption process. Adsorption capacity increased from 17.86 mg g^{-1} in corncob to 60.82 mg g^{-1} in FCC and 206.67 mg g^{-1} in CCNC implying CCNC had the highest adsorption quality. The rate of adsorption was most accurately predicted by pseudo first order kinetics. Adsorption mechanism was governed by film diffusion with contribution from intra-particle diffusion. Adsorption process was spontaneous ($-\Delta G^o$) at all temperatures (303–315 K), exothermic ($-\Delta H^o$) and physical on CC (3.73 kJ mol^{-1}) and CCNC (3.42 kJ mol^{-1}) however it was endothermic ($+\Delta H^o$) and chemical on FCC (12.86 kJ mol^{-1}). This study shows that CCNC is comparatively the best adsorbent with highest adsorption capacity.

Keywords Cellulose nanostructure · Corncob morphological characteristics · Acid functionalization · Langmuir adsorption model · Methyl orange removal

1 Introduction

Nanostructured materials are prominently emerging as distinct adsorbents for remediation of wastewater containing heavy metals, organic pollutants and dyes [1–3]. They are better than macro-adsorbents because they possess characteristics such as improved and enhanced reactive binding sites in addition to higher adsorption capacities more suitable for environmental remediation. Recent developments in nanotechnology suggest that water quality problems caused by any class of pollutants could be solved using nano-based materials owing to their greater adsorption capacities associated with their morphology [4–9].

Recently, application of nanostructured materials such as nanocellulose and nanoparticles have surged due to their distinct characteristics of large surface area and vastly reactive sites. Moreover, the retention of intrinsic regenerative and chemical properties of cellulose though

✉ Luqmon Azeez, luqman.azeez@uniosun.edu.ng | [1]Department of Mechanical Engineering, Osun State University, Osogbo, Nigeria. [2]Department of Pure and Applied Chemistry, Osun State University, Osogbo, Nigeria. [3]Department of Science Laboratory Technology, Federal Polytechnic Ilaro, Ilaro, Nigeria. [4]Department of Chemical Engineering, University of Ilorin, Ilorin, Nigeria.

enhanced in nanocellulose is also an advantage [1, 6, 10, 11].

Many studies have demonstrated the effectiveness of nanoparticles for the removal and remediation of pollutants in wastewater. Nanoparticles such as zero-valent silver, zero-valent iron, gold, magnetite, multi-walled carbon nanotube, MgO, NiO, TiO_2, cobalt ferrite nanoparticles and iron oxide/carbon nanocomposites, γ-Fe_2O_3/SiO_2/chitosan composite, nanoporous core–shell $Cu@Cu_2O$ nanocomposite and ultrasonic aided nanoparticle stacked activated carbons have previously been deployed as adsorbents to remediate wastewater containing different pollutants with note-worthy results [3, 8, 12–21].

However, limited abundance, lack of sustainability, toxicity, cost-effectiveness and possible environmental distress arising from their application are causes of concerns. Though, biologically synthesized nanoparticles are less toxic yet renewability of source materials is a basis of apprehension.

Cellulose is the most abundant inexhaustible renewable biodegradable biopolymer. It is a biocompatible polysaccharide compound consisting of two regions; crystalline and amorphous. It is a homopolymer of glucose composed of glucopyranosyl units linked together by 1–4 β glycosidic bond [9–11, 22–24].

Nanocellulose is a non-hazardous, biodegradable, low-weight, highly reactive and thermally stable nano-scale material synthesized by disruption of amorphous region of the cellulose into nanocrystals or nanofibrils. They equally have attributes of broad surface functionality, large surface area, high surface tension and high crystallinity degree. Combination of these properties makes nanocellulose promising and unique adsorbents in addition to other useful applications in biomedical, pharmaceutical, construction and chemical industries [2, 6, 7, 25, 26].

Nanocelluose can be extracted from lignocellulose using a number of processes each with its advantages and disadvantages. Treatments involving chemicals (acid hydrolysis, 2,2,6,6-tetramethylpiperidine-1-oxyl (TEMPO) oxidation), mechanical/physical (crushing, grinding, homogenization, extrusion) and biological (enzyme hydrolysis) processes are most common methods of nanocellulose synthesis [1, 4, 9, 10, 23, 24].

In acid hydrolysis, the amorphous region which is susceptible to acid attack is hydrolysed while the crystalline region remains intact. It introduces sulphate ester group onto the nanocellulose which improves its adsorbing ability. Nanocellulose extracted by acid hydrolysis is extremely hydrophilic, chiral, mechanically strong, biocompatible and has uniform particle size as well as wide-ranging chemical-modifying capacity [10, 11, 27].

Another method of enhancing the adsorptive capacity of adsorbent is activation/functionalization with acids, alkali and salts. This majorly modifies the biological structure, cleaves the bond, influences pyrolytic decomposition, improves thermal resistance and inhibits tar formation [28–30]. Acid functionalization with H_3PO_4 induces physical, and chemical modification, reforms formation of cross-linked structure, develops micropores, enhances surface adsorptive properties by increasing their percentage carbon contents via reduction of water content and burning-off of volatile solids arising from breakage of cellulosic materials [31–37].

Corncob is an agricultural waste generated during the processing of corn in huge quantity which disposal invariably creates environmental burden because most farmers prefer to burn it off. Therefore, its application as raw or modified adsorbent is highly encouraged as it will reduce the burden of burning-off resulting in environmental pollution of air and water. It is an inexpensive and environmentally friendly effective adsorbent which has been applied to remediate heavy metals, dyes, and crude-oil polluted water. It has also found application in the reinforcement of polyvinyl alcohol membrane [11, 29, 38].

Methyl orange (MO) is an anionic azo dye which is useful as a titrimetric indicator in the laboratories as well as for textile dyeing and paper printing. Although, it has vast versatility but its low biodegradability, recalcitrance in the environment, chemical stability, carcinogenic potentials and secondary metabolic intermediates are sources of worries [20, 39, 40]. Dyes are highly water soluble, stable to photo-degradation, non-biodegradable and have complex structure. Once their effluents are discharged into the environment, they disrupt ecological, biological and chemical processes. Epidemiological studies have linked discharge of dye effluents with adverse effects on human and animal health [21, 26, 38, 41, 42]. It thus becomes obligatory from aforementioned impacts for effluents containing MO be treated before their discharge into the environment.

This study was aimed at synthesizing nanostructured and functionalized corncob using hydrolysis techniques for their application as suitable adsorbents for MO removal from simulated wastewater.

2 Materials and methods

2.1 Reagents

NaOH, H_2SO_4, H_3PO_4, methyl orange (λ_{max} 480 nm) used in the study are of analytical grade from Sigma-Aldrich, Germany.

2.2 Adsorbent collection and synthesis

Corncobs (CC) were collected from a local agricultural farm in Osogbo, Osun State, cut into pieces, dried in an oven at 80 °C to complete dryness, pulverized into powder and sieved to 102 μm particle size.

2.3 Synthesis of corncob nanocellulose by acid hydrolysis (CCNC)

Removal of lignin and hemicellulose was done by dissolving powder corncob in 5% NaOH and stirred for 4 h to obtain a homogenous suspension that was washed continuously with deionized water until the pH was 6.5. The suspension was filtered and the filtrate dried at 80 °C for 24 h.

Exactly 100 g of NaOH-treated corncob was added to 60% H_2SO_4. The suspension was stirred for 2 h for thorough mixing at 45 °C. The pH of the suspension was adjusted to 6.5 by washing with deionized water, centrifuged at 5000 rpm for 20 min and dried at 80 °C to obtain nanocellulose powder.

2.4 Functionalization of corncob (FCC)

The functionalization was carried out by chemically treating 20 g of the sieved corncob with 250 mL H_3PO_4 and heated on the magnetic stirrer at 100 °C until a paste was completely formed. The pH of functionalized corncob was brought to 6 by washing the paste with deionized water which was afterwards dried in an oven at 105 °C.

2.5 Characterization of raw, nanocellulose and functionalized corncob

Surface chemistry was characterized by Fourier transform infrared spectroscopy (FTIR) (Model 500, Buck Scientific Inc.) in the range of 400–4000 cm^{-1}. Morphology and elemental composition were characterized by scanning electron microscopy (SEM) and energy dispersive X-ray (Bruker-X Flash 6130, Carl Zeiss, EVO 18 Research, Germany).

2.6 Methyl orange preparation and pH point of zero charge

A stock solution of 50 mg L^{-1} methyl orange (MO) was used for the adsorption study. The pH point of zero charge (pH$_{pzc}$) was determined by adding 0.1 g of each adsorbent to 200 mL solution of 0.1 M NaCl of known initial pH. The pH was adjusted with 0.1 M NaOH or 0.1 M HCl to pH 2–8. The conical flasks were sealed and placed on a shaker for 24 h after which the final pH was measured with Jenway 6405 pH meter (Germany).

2.7 Batch adsorption studies

Effects of different operational factors on adsorption of MO on the three adsorbents were studied. Batch adsorption was carried out by adding 0.5 g of each adsorbent to 50 mg L^{-1} MO, agitated for 30 min at 303 K in a thermostat regulated water bath with shaker (Uniscope water bath shaker) operated at 300 rpm. Absorbance readings were recorded with Jenway 6405 UV–visible Spectrophotometer (Buch Scientific Inc. USA) at 480 nm. Other adsorption investigations were achieved by varying initial solution pH (2–8, adjusted with 0.1 M HCl or NaOH), initial concentration of MO (10–50 mg L^{-1}), adsorbent dosage (0.1–0.5 g), contact time (0–75 min) and temperature (303–315 K) to accomplish best removal conditions required for MO. Percentage MO removal and quantity adsorbed at equilibrium were calculated using Eqs. 1 and 2 respectively.

$$\%MO\ removal = \frac{(C_i - C_f) \times 100}{C_i} \qquad (1)$$

$$q_e = \frac{(C_i - C_e)V}{M} \qquad (2)$$

where q_e is amount of MO adsorbed per unit mass of adsorbent (mg g^{-1}) at equilibrium, C_i is the initial MO concentration (mg L^{-1}), C_f is the final MO concentration (mg L^{-1}), C_e is the concentration of MO remaining at equilibrium, V = volume of MO solution (L) and M = mass of adsorbent (g).

2.8 Adsorption isotherms, kinetics and thermodynamics

Four adsorption isotherms (Langmuir, Freundlich, Tempkin and Dubinin–Radushkevich) [43–46] were applied to evaluate the adsorption behaviour between MO and adsorbents as listed in Table 1.

Three kinetic models listed in Table 1 viz. pseudo first order, pseudo second order and Elovich were employed to describe the kinetics of adsorption of MO on adsorbents. Adsorption mechanisms were studied using equations listed in Table 1 for intra-particle diffusion and film diffusion. The predictability of each model for the description of kinetics was validated with correlation coefficient (R^2) and non-linear Chi square test (Eq. 3).

Spontaneity and energetics of interaction between MO and adsorbents were evaluated from the plot obtained from equations of thermodynamics in Table 1.

Table 1 Adsorption isotherm, kinetic and thermodynamic parameters equations

Model	Type and reference	Model expression and constants
Adsorption isotherm	Langmuir [43]	$\frac{C_e}{q_e} = \frac{C_e}{q_{max}} + \frac{1}{q_{max}K_L}$
		$R_L = \frac{1}{1+K_L C_o}$
	Freundlich [44]	$log q_e = \frac{1}{n} log C_e + log K_f$
	Temkin, Temkin and Pyzhev [45]	$q_e = B ln A + B ln C_e$
		$B = {RT}/{b}$
	Dubinin–Radushkevich, Dubinin and Radushkevich [46]	$ln q_e = ln q_o - \beta \varepsilon^2$
		$\varepsilon = RT ln \left(1 + \frac{1}{C_e}\right)$
		$E = \sqrt{{1}/{2\beta}}$
Kinetics	Pseudo first order	$ln(q_e - q_t) = ln q_e - K_1 t$
	Pseudo second order	$\frac{t}{q_t} = \frac{1}{K_2 q_e^2} + \frac{t}{q_e}$
	Elovich	$q_t = \frac{1}{\beta} ln(\alpha\beta) + \frac{1}{\beta} ln t$
	Intra-particle diffusion	$q_t = K_{diff} t^{1/2} + C$
	Film diffusion (Boyd model)	$F = \frac{q_t}{q_e}$
		$B_t = -0.4977 - ln(1 - F)$
Thermodynamics		$ln K_o = \frac{\Delta S^o}{R} - \frac{\Delta H^o}{RT}$
		$\Delta G^o = -RT ln K_o$

C_e is the equilibrium concentration of methyl orange dye (mg L^{-1}), q_e is the quantity of methyl orange dye adsorbed onto the CC, FCC and CCNC at equilibrium (mg g^{-1}), q_{max} is the maximum monolayer adsorption capacity of adsorbent (mg g^{-1}) and K_L is the Langmuir adsorption constant (L mg^{-1}). K_f and n are Freundlich constants. A (L g^{-1}) and B are Tempkin isotherm and Tempkin constants. T is the absolute temperature (K), and R is the gas constant. E is energy of adsorption. q_t is the quantity absorbed at time t (mg g^{-1}) and K_1 is the rate constant for the pseudo first order sorption in min^{-1}. K_2 is the rate constant of the pseudo second order kinetic model in g mg^{-1} min^{-1}. α and β are constants depicting chemisorption rate and the extent of surface coverage. ΔS^o is change in entropy, ΔH^o is change in enthalpy and ΔG^o, change in free energy

$$\chi^2 = \sum_{i=1}^{n} \frac{(q_{exp} - q_{cal})^2}{q_{cal}} \qquad (3)$$

2.9 Regeneration studies

Exactly 0.1 g each of CC, FCC and CCNC was added separately to 50 mL of 50 mg L^{-1} MO in a 250 mL flask. The solution was adjusted to pH 3.01, 4.11 and 2.09 (pH at which maximum adsorption occurred for each) for CC, FCC and CCNC respectively and agitated for 1 h. Thereafter, adsorption solutions were centrifuged at 300 rpm for 30 min and residual MO concentration was determined at 480 nm. Methyl orange-loaded adsorbents were washed with water, dried at 70 °C to complete dryness and was afterwards soaked in 100 mL of water for desorption process. This mixture was shaken vigorously for 30 min, centrifuged and desorbed MO concentration from methyl orange loaded adsorbents was determined. Percentage desorption was calculated with Eq. 4

$$Percentage\ desorption = \frac{quantity\ of\ dye\ desorbed\ by\ water}{quantity\ adsorbed\ during\ loading} \times 100 \qquad (4)$$

3 Results and discussion

3.1 Characterization of CC, FCC and CCNC

3.1.1 Surface chemistry of CC, FCC and CCNC

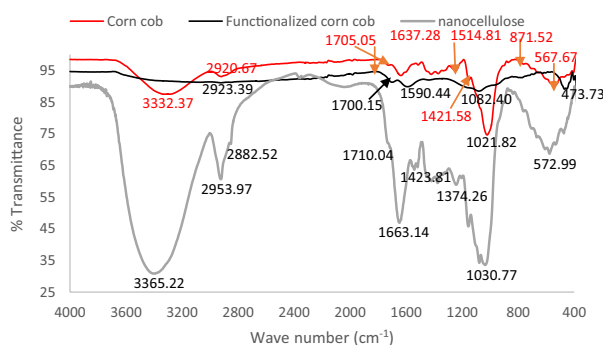Investigation of functional groups present on the surfaces of adsorbents was done and presented in Fig. 1.

Fig. 1 FTIR spectra of corncob, functionalized corncob and nanocellulose

Differences in surface functional groups in corncob (CC), functionalized corncob (FCC) and corncob nanocellulose (CCNC) were investigated using FTIR. Spectra of CC and CCNC reveal peaks at 3327.37 and 3365.22 cm^{-1} showing the presence of O–H group whereas it was absent in FCC. Bands between 2920.67 and 2953.97 cm^{-1} in all adsorbents correspond to methyl C–H while peaks between 1705.05 and 1710.04 cm^{-1} are assigned to C=O. Peaks between 1637.28 and 1663.14 cm^{-1} result from bending vibrations of O–H, at 1514.81–1590.44 cm^{-1} from residual hemicellulose, 1421.58–1423.81 cm^{-1} from CH$_2$ of cellulose crystal I, 1021.82–1030.77 and 857.22–871.52 cm^{-1} from PO$_4^{3-}$, SO$_4^{2-}$ and C–O–C of β-glycosidic linkages. The peaks obtained in this study for CC and CCNC have previously been affirmed as peaks representative of cellulose and nanocellulose [10, 11, 26].

Absence of O–H in FCC is attributable to the activation with H$_3$PO$_4$ as it has been previously reported that acid functionalization reduces/removes water moieties leading to continuing loss of OH and thus creating cavities good enough for adsorption [47, 48].

The presence of these characteristic peaks in these adsorbents demonstrate their involvement in the adsorption process. Adsorption process is a surface phenomenon that is dependent on the surface chemistry and characteristic pores. The presence of these functional groups on adsorbents' surfaces would enhance electrostatic interactions of adsorbent–adsorbate and would play important role in the adsorption of MO [42, 49]. These functional groups have been found to be responsible for removal of dyes in other studies via formation of covalent bonds and matrix between active sites on adsorbents and adsorbates [38, 50].

The existence and appearance of nearly all functional groups of nanocellulose in corncob is an indication of non-destructive retention of intrinsic chemical properties although some peaks were more intense. Chemical characteristics in CCNC compared to CC were not significantly altered as in contrast to FCC. These agree with studies of Liu et al. [27] and Yang et al. [11].

3.2 Morphological and elemental characteristics of CC, FCC and CCNC

Scanning electron micrograph (SEM) of CC (Fig. 2a) shows a strictly compressed nearly non-porous rod-like shapes with uneven particle surfaces having average size 248.72 ± 124.37 μm. SEM of FCC (Fig. 2b) reveals a greatly developed, highly porous with clear-cut cavities that could facilitate adsorption. Its pores have average size of 27.40 ± 14.31 μm. SEM of CCNC (Fig. 2c) shows uneven rhombic-like structure having crystalline smaller particles with average size 5.25 ± 1.39 μm. Smallest particle

sizes in synthesized nanocellulose is an indication of its nanostructure which offer better adsorption performance than macro-aggregated structure. Well-developed pores and rougher cavities in SEM of FCC are connected with loss of volatile materials especially water and breakdown of cellulosic materials resulting in well-built cavities coupled with gasification of phosphorus species impregnated with H$_3$PO$_4$ in FCC leading to the expansion of pores. These results are consistent with reports that expansion of porosity is related to amount of phosphorus [29, 30, 35–37]. Since adsorption process is a surface occurrence, adsorbent quality will be functions of number and nature of pores [41, 42]. As obtained for SEM in this study, it indicates CCNC had best qualities for uptake of MO as it has been previously reported that rough surfaces with developed cavities are more favourable for adsorption of pollutants [29, 49].

EDX analysis was used to reveal elemental compositions and percentages of prominent elements present in the three adsorbents (Table 2). Percentage of carbon content increased by 41.42% in FCC and decreased by 71.13% in CCNC over CC. There were reductions of 31.87 and 18.69% in percentage oxygen contents in FCC and CCNC compared with CC. Presence of phosphorus (3.81%) in FCC and sulphur (17.24%) in addition to sodium (21.65%) in CCNC was obtained. Percentage of carbon in an adsorbent is directly linked to its adsorption property and as obtained in this study for FCC, it has highest carbon content stemming possibly from a reduction in water content, burning-off volatile materials and release of tar from cellulosic material produced by functionalization with H$_3$PO$_4$. Existence of P in FCC, S and Na in CCNC is a confirmation of their synthetic routes [33, 34, 37].

3.3 Batch equilibrium experiments

pH point of zero charge (pH$_{pzc}$) for CC, FCC and CCNC occurred at 4.82, 4.91 and 5.25 respectively (Fig. 3) indicating adsorption of MO would be maximally effective below these pH values due to the fact that the surfaces of these adsorbents would be cationic and optimum removal of MO (anionic dye) would be achieved. Maximum adsorption of MO on CC, FCC and CCNC occurred at pH 3.01, 4.11 and 2.09 respectively (Fig. 4). Initial increase in percentage MO removal with an increase in pH from 2 to 4 followed by a gradual decrease in percentage as it increased from 4 to 8 was recorded. Adsorption studies were consequently carried out at respective maximum pH of adsorbents. pH facilitates and influences the mobility of the adsorbate on adsorbent. The surface of adsorbent is cationic at pH < pH$_{pzc}$ whereas it is anionic at pH > pH$_{pzc}$. pH$_{pzc}$ plays an effective role in determining the electrostatic surface charge on adsorbent needed for optimum adsorption of

Fig. 2 SEM and EDX images of **a** Corncob, **b** functionalized corncob, **c** nanocellulose
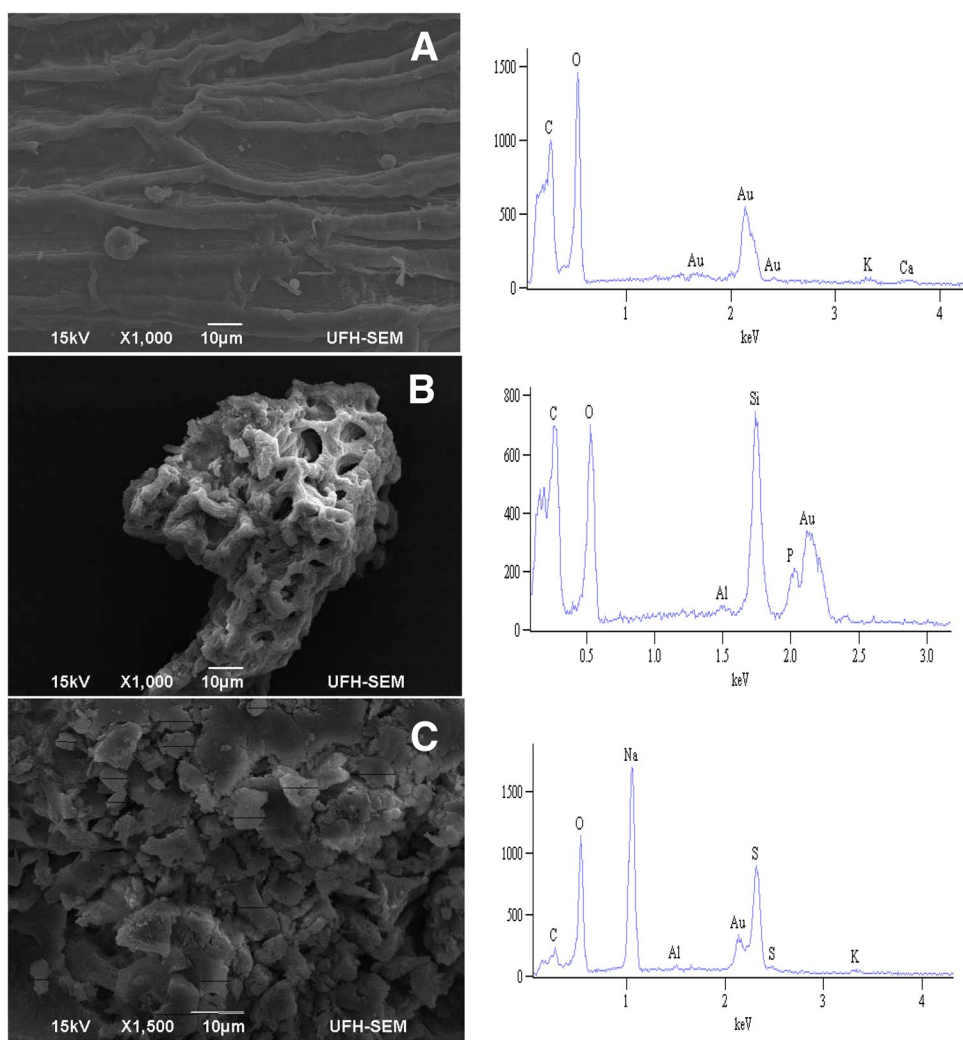

Table 2 Elemental compositions of corncob, functionalized corncob and corncob nanocellulose

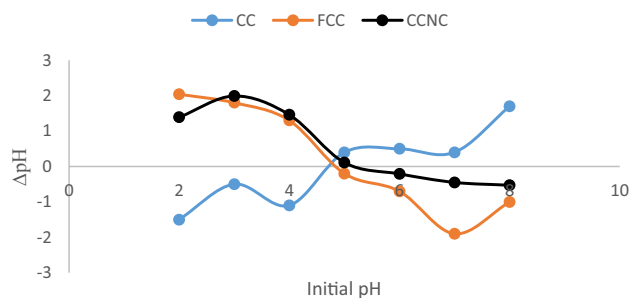| Element	Weight percentage (%)		
	CC	FCC	CCNC
C	17.19	24.31	4.89
O	25.57	17.42	20.79
Si	–	10.36	–
Al	–	0.32	0.39
Na	–	–	21.65
S	–	–	17.24
K	0.96	–	0.75
Ca	0.98	–	–
P	–	3.81	–

Fig. 3 pH point of zero charge (pH_{pzc}) plot of corncob, functionalized corncob and nanocellulose

the adsorbate. It influences adsorbent surface charge and dissociation of functional groups responsible for adsorption [2, 6, 8]. Maximum adsorption results at $pH < pH_{pzc}$ for all adsorbents in this study are consistent with the anionic nature of adsorbate and surface charges (cationic) of the adsorbent. Sorption of adsorbate is hinged on adsorbent surface charges/chemistry and influence of pH on the mobility of adsorbate [47, 51].

Percentage adsorption of MO increased with increase in the concentration of MO ranging from least (10 mg L^{-1}) to highest concentration (50 mg L^{-1}) of MO obtained
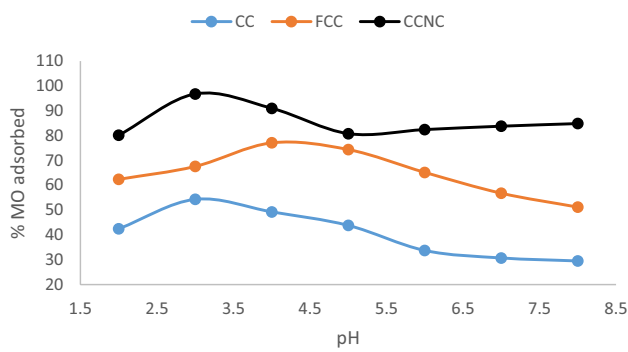
Fig. 4 Effects of pH on percentage adsorption of methyl orange

are 40.36–66.91% for CC, 59.39–87.27% for FCC and 54.74–95.62 for CCNC respectively. These increases in percentage MO adsorbed are related to superior driving forces to overcome mass transfer impediments as the concentration increased hence this trend as has been previously reported as findings by Adekola et al. [47] and Abdelwahab and Amin [52].

A direct relationship between dosage and percentage adsorption was obtained; the higher the dosage, the more improved the adsorption was. Percentage adsorption with respect to dosage from least (0.1 g) to highest (0.5 g) follows CCNC (80.08–96.53%) > FCC (70.79–91.92%) > CC (32.71–48.13%). This is associated with more active sites in higher dosage available to the same concentration and volume of dye molecules, thus, the increase in percentage adsorption. More so, higher adsorption percentage recorded for FCC and CCNC could be connected to more reactive sites and larger pores in CCNC and FCC. Similar experimental trend was obtained by Chan et al. [2], Ojedokun and Bello [29], Ojo et al. [30] and Saravanan et al. [38].

Quantity of MO adsorbed (q_t) at different time interval (Fig. 5) was firstly promptly swift with time but gradually attained equilibrium at 50, 35 and 30 min for CC, FCC and CCNC respectively. q_t increased from 5.12 to 27.97 mg g^{-1},
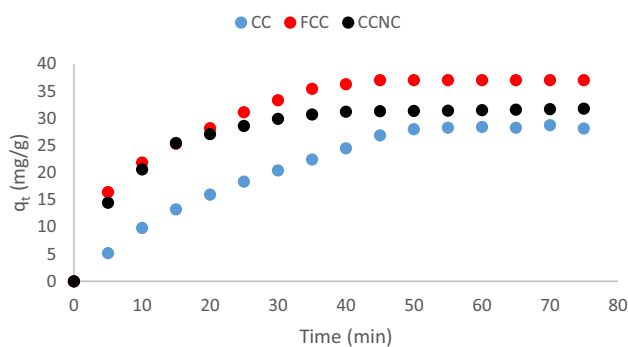

Fig. 5 Quantity of MO adsorbed by corncob, functionalized corncob and nanocellulose at different contact time

16.44 to 35.44 mg g^{-1} and 14.48 to 29.9 mg g^{-1} for CC, FCC and CCNC respectively. The behaviour of adsorbent–adsorbate relationship with respect to time shows a robustly swift removal at the initial stage that became gradual as adsorption reached equilibrium. The initial prompt rise in q_t is attributable to availability of reactive sites on adsorbents that were occupied as time progressed and this is consistent with reports of Adekola et al. [47] Inyinbor et al. [53, 54] and Huang et al. [39].

The dependence of adsorption on temperature for uptake of MO was carried out between 303 and 315 K. Percentage removal of MO reduced with increase in temperature for CC from 18.96 to 15.76% and 89.14 to 78.74% for CCNC while it increased from 45.94 to 78.68% for FCC. Reductions in percentage removal of MO with temperature on CC and CCNC signify exothermic nature whereas adsorption was endothermic on FCC. Exothermic adsorption process is indicative of weak binding/sorptive forces governing the mobility of adsorbate onto adsorbents at different temperatures while endothermic nature in FCC might be associated with increased mobility of MO onto FCC. Similar observations were reported by Inyinbor et al. [53] and Ojedokun and Bello [29].

3.4 Adsorption isotherms studies on CC, FCC and CCNC

This study investigated the suitability and fitting of parameters of adsorption to four isothermal models: Langmuir, Freundlich, Temkin and Dubinin–Radushkevich and results presented in Table 3. The appropriateness of each model was determined with the correlation coefficient (R^2); the

Table 3 Adsorption isotherm parameters for the uptake of MO on different adsorbents at 303 K

Isotherms	Constants	CC	FCC	CCNC
Langmuir	q_{max} (mg g^{-1})	17.86	60.82	206.67
	K_L (L mg^{-1})	0.951	0.687	0.250
	R_L	0.021	0.012	0.074
	R^2	0.970	0.920	0.991
Freundlich	n	2.08	3.02	3.43
	K_f	21.04	58.45	66.23
	R^2	0.664	0.873	0.982
Temkin	B	142.47	331.07	33.76
	A (L g^{-1})	3.09	14.25	1.055
	b (J mol^{-1})	17.68	7.61	16.14
	R^2	0.626	0.751	0.903
Dubinin–Radushkevich	q_o (mg g^{-1})	670.44	1609.75	882.05
	$\beta \times 10^{-6}$ (mol^2 K^{-1} J^{-2})	3.58	3.02	1.08
	E (kJ mol^{-1})	3.73	12.86	3.42
	R^2	0.922	0.649	0.853

higher it is, the more appropriate the fittingness of the model.

Correlation coefficients for the three adsorbents in each model follows Langmuir (R^2_{CC}—0.970, R^2_{FCC}—0.920, R^2_{CCNC}—0.991) > Freundlich (R^2_{CC}—0.664, R^2_{FCC}—0.873, R^2_{CCNC}—0.982) > Temkin (R^2_{CC}—0.626, R^2_{FCC}—0.751, R^2_{CCNC}—0.903) > Dubinin–Radushkevich (R^2_{CC}—0.922, R^2_{FCC}—0.649, R^2_{CCNC}—0.53). Langmuir (Fig. 6) was the most appropriate model best fitted to parameters of adsorption indicating adsorption of MO was on monolayer uniform surfaces of CC, FCC and CCNC.

Maximum monolayer adsorption capacity (q_{max}) of 17.86, 60.82 and 206.67 mg g^{-1} were calculated for CC, FCC and CCNC respectively. q_{max} values of adsorbents in this study are compared with nanostructured and functionalized adsorbents previously reported (Table 4). In terms of performance, CCNC out performed some of the

adsorbents listed implying its excellent suitability for dye removal.

The favourability of adsorption study is deduced from the values of R_L ranging between $0 < R_L < 1$. In this study, R_L was found to be 0.021, 0.012 and 0.074 for CC, FCC and CCNC respectively which is indicative of favourability of adsorption processes on the three adsorbents [8].

Constants K_F and from Freundlich isotherm model are used to explain favourable or cooperative process of adsorption when is greater or lower than 1 while a relatively high value of K_F in comparison with other adsorbents favours higher adsorption capacity. CC, FCC and CCNC have values of 2.98, 3.02 and 3.43 indicating favourable adsorption which equally supports the findings of R_L. It also validates q_{max} values as adsorption was most intense on CCNC with the highest value of . K_F range follows CCNC > FCC > CC indicating highest removal of MO was by CCNC [2, 58].

Tempkin isotherm sorption binding constant was highest in FCC followed by CC and CCNC signifying the decrease in the involvement of chemical adsorption during the uptake of MO [53, 54].

Characteristics of adsorbents as related to porosity and energy of adsorption were calculated from Dubinin–Radushkevich isotherm. Energies of adsorption are 3.73, 12.86 and 3.42 kJ mol^{-1} for CC, FCC and CCNC respectively suggesting physical adsorption with respect to CC and CCNC while the adsorption was chemical on FCC [29, 30].
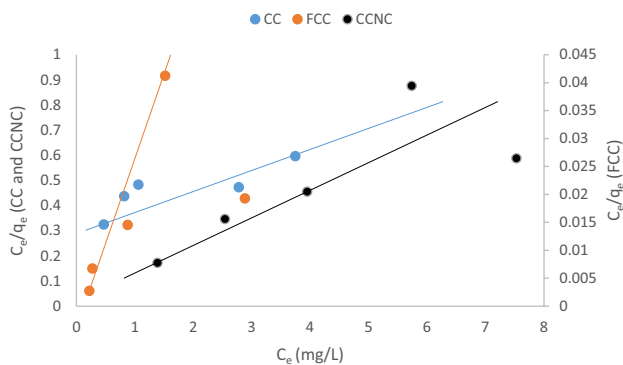
3.5 Adsorption kinetics and mechanism of MO on RH and FRH

Adsorption is either exclusively controlled by the rate of uptake of adsorbate on adsorbent or combination of rate

Fig. 6 Langmuir isotherm plot for the adsorption of MO on different adsorbents. Scale—FCC × 10

Table 4 Comparative assessment of dye removal capacities of nanostructured and functionalized adsorbents

Adsorbent	q_{max} (mg g^{-1})	Pollutant	Reference
H$_3$PO$_4$-functionalized corncob	50.00	Congo red	Ojedokun and Bello [29]
H$_3$PO$_4$-functionalized wall nut shell	40	Congo red	Ojo et al. [30]
H$_3$PO$_4$-activated cotton fibre	476.19	Methylene blue	Duan et al. [33]
Nanocellulose (cellulose fibre)	118	Methylene blue	Batmaz et al. [6]
Cellulose nanocrystals	122.2	Methylene blue	Chen et al. [23]
Nanocrystalline cellulose	101.16	Methylene blue	He et al. [55]
Acid modified carbon coated monolith	147.06	Methyl orange	Willie et al. [56]
De-oiled biomass	9.9	Fuchsin dye	Renita et al. [41]
H$_2$SO$_4$-modified *Enteromorpha intestinalis*	95.27	Methylene blue	Saravanan et al. [38]
Microwave assisted sawdust	58.14	Methylene blue	Suganya et al. [57]
Modified *Pinus wallichiana*	456.23	Malachite green	Gautam et al. [21]
Microwave-assisted corncob carbon	82.71	Methylene blue	Tharaneedhar et al. [42]
Corncob	17.86	Methyl orange	This study
H$_3$PO$_4$-functionalized corncob	60.82	Methyl orange	This study
Nanostructured corncob	206.67	Methyl orange	This study

Table 5 Adsorption kinetics of MO on the three adsorbents

	Constants	CC	FCC	CCNC
	$q_{e\ experimental}$ (mg g^{-1})	30.27	37.01	31.30
Pseudo first order	$q_{e,\ calculated}$ (mg g^{-1})	37.34	36.29	27.39
	K_1 (min^{-1})	0.052	0.088	0.097
	R^2	0.987	0.996	0.993
	χ^2	1.336	0.014	0.556
Pseudo second order	$q_{e,\ calculated}$ (mg g^{-1})	43.58	42.05	15.64
	$K_2 \times 10^{-3}$ (g mg^{-1} min^{-1})	0.68	2.89	1.46
	R^2	0.976	0.950	0.794
	χ^2	4.064	0.603	1.167
Elovich	α (mg g^{-1} min^{-1})	2.838	13.221	20.796
	β (g mg^{-1})	0.102	0.121	0.164
	R^2	0.976	0.952	0.908
Intra-particle diffusion	K_{1diff} (mg g^{-1} min$^{-1/2}$)	4.76	5.12	4.73
	K_{2diff} (mg g^{-1} min$^{-1/2}$)	0.0036	0.004	0.24
	R_1^2	0.998	0.995	0.903
	R_2^2	0.943	0.907	0.844

of adsorbate on active sites and diffusion mechanisms [30, 50, 59]. Hence, the mechanism and rate of adsorption were studied for the adsorption of MO on CC, FCC and CCNC. The description of rate and mechanistic pathway of adsorption of MO on CC, FCC and CCNC (Table 5) in order of correlation coefficients follow the trend pseudo first order (R_{CC}^2—0.987, R_{FCC}^2—0.996 and R_{CCNC}^2—0.993) > pseudo second order (R_{CC}^2—0.976, R_{FCC}^2—0.950 and R_{CCNC}^2—0.794) > Elovich (R_{CC}^2—0.976, R_{FCC}^2—0.952 and R_{CCNC}^2—0.908). Calculated quantity adsorbed at equilibrium (q_e) for pseudo first order kinetics is the closest to the experimental q_e coupled with lowest values χ^2.

Pseudo first order kinetics (Fig. 7) with highest R^2, lowest χ^2 and closest q_e calculated to q_e experimental was the most accurate and precise to describe the rate of adsorption of MO on all adsorbents indicating a monomolecular layer of MO on CC, FCC and CCNC [1, 6, 57].

Adsorption mechanisms that explain the effects of mass transfer resistance on the adsorption of MO on different adsorbents were studied with intra-particle diffusion and film diffusion. Adsorption mechanism may involve film, surface and intra-particle diffusion taking place independently or concurrently [38]. Intra-particle diffusion displays a two-layer stage: rapid (first) describing the rate controlling steps and steady (second)—describes the rate limiting step (Fig. 8). The first rapid part provides the information about diffusion of MO onto the surfaces of adsorbents while the second steady part indicates predominance of intra-particle diffusion [58]. Two-stage plots and deviations from origin suggest that intra-particular diffusion mechanism was involved in adsorption process but not the sole rate-determining step [8, 50, 57]. Higher values of K_{1diff}
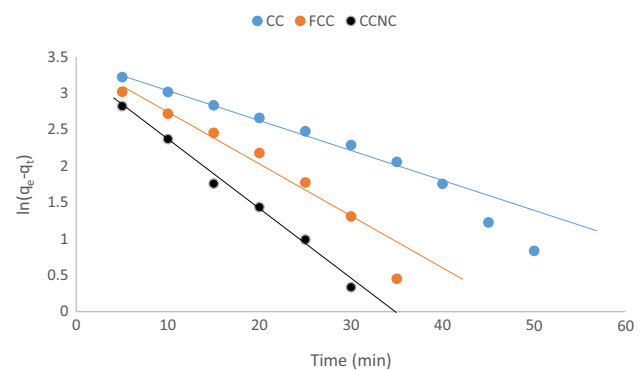
Fig. 7 Pseudo first order kinetics plot of corncob, functionalized corncob and nanocellulose for MO removal
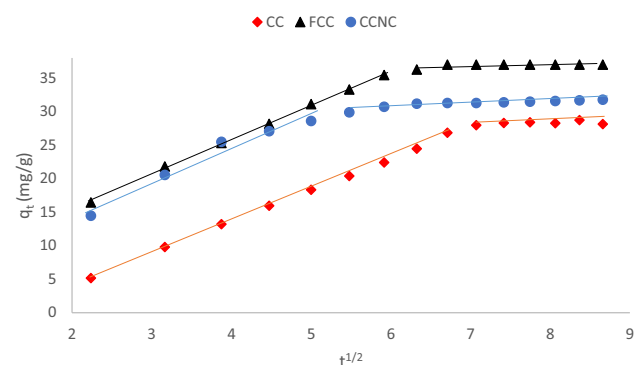
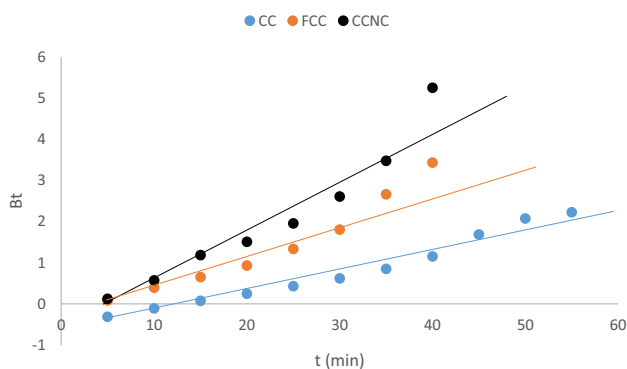**Fig. 8** Intra-particle diffusion plot of corncob, functionalized corncob and nanocellulose for MO removal

Fig. 9 Boyd plot for the removal of MO on corncob, functionalized corncob and nanocellulose
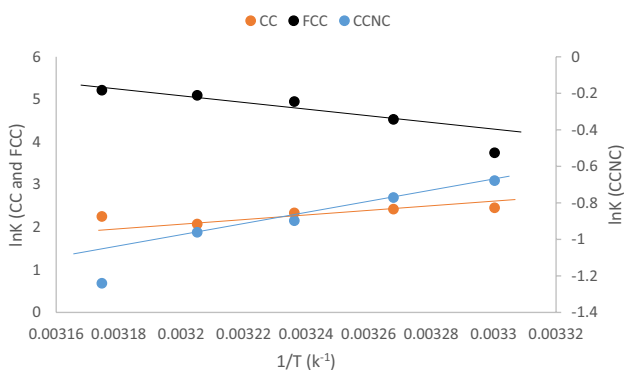

Fig. 10 Van't Hoff's plot of MO adsorption on corncob, functionalized corncob and nanocellulose

over K_{2diff} is an indication of greater driving force in the first part than second [58]. The thickness of boundary (Table 5) follows FCC > CCNC > CC implying the contribution of boundary layer diffusion during the adsorption process. The thicker the boundary, the greater the boundary diffusion effects which was most pronounced in FCC [8, 50]. The Boyd plot (Fig. 9) used to predict adsorption mechanism shows that film diffusion was the rate-controlling step as no line passed through the origin. This is in consonance with reports of Azeez et al. [8] and Oyelude et al. [50].

3.6 Adsorption thermodynamics

Thermodynamic parameters were evaluated from the plot of Van't Hoff (Fig. 10). The values of ΔG^o, ΔH^o and ΔS^o for adsorption of MO on CC, FCC and CCNC are presented in Table 6.

ΔH^o and ΔS^o were negative for CC and CCNC while they were positive for FCC. ΔG^o values were negative for all adsorbents increasing with increasing temperature for CC and CCNC whereas they decreased with increasing temperature for FCC. ΔG^o ranges from -6.21 to -5.65 kJ mol^{-1} for CC, -10.08 to -14.16 kJ mol^{-1} for FCC and -31.13 to -30.98 kJ mol^{-1} for CCNC.

The nature of energy associated with the adsorption process as well as feasibility/spontaneity are determined with deductions from thermodynamic parameters. Negative values of ΔH^o and ΔS^o for adsorption of MO on CC and CCNC imply exothermic nature and manifestation of high degree of randomness was involved during adsorption process suggesting direct affinity of CC and CCNC for MO [38, 41, 42]. In contrast, removal of MO was endothermic on FCC as indicated by positive values of ΔH^o and ΔS^o signifying indirect affinity for MO [29, 30]. Adsorption on all adsorbents was favourably feasible as revealed by values of ΔG^o decreasing with increase in temperature for FCC while it increased with increasing temperature for CC and CCNC. This is in agreement with reports of Tharaneedhar et al. [42]. Differences in energy natures and affinities of adsorbents could be linked to the modification of surface chemistry and reduction in particle sizes [29, 47, 55, 60].

3.7 Regeneration/desorption studies of MO from CC, FCC and CCNC

Percentage desorption ranges in order CC (87.13%) > CCNC (80.74%) > FCC (65.23%). With over 80% desorption, it indicates that CC and CCNC can be easily regenerated for more adsorption processes. Relatively higher desorption percentages obtained for CC and CCNC imply MO was weakly bonded onto CC and CCNC. This is consonance with energy of adsorption which indicate physiosorption while relatively lower desorption percentage of FCC indicates MO strongly bonded to FCC suggesting chemical adsorption process. Similar results were reported by Inyinbor et al. [53, 54] and Olajire et al. [58].

Table 6 Thermodynamic parameters of MO adsorption

Adsorbent	ΔH^o (kJ mol^{-1})	ΔS^o (J K^{-1} mol^{-1})	ΔG^o (kJ mol^{-1})				
			303 K	306 K	309 K	312 K	315 K
CC	-20.340	-46.639	-6.209	-6.069	-5.929	-5.789	-5.649
FCC	92.894	339.84	-10.077	-11.097	-12.117	-13.136	-14.156
CCNC	-34.705	-11.814	-31.125	-31.090	-31.054	-31.019	-30.983

4 Conclusion

This study has described and reported the characterization of nanostructured and functionalized corncob via acid hydrolysis as adsorbents for MO uptake. Acid functionalization greatly influenced surface chemistry and morphology whereas nanocellulose had similar surface chemistry comparable to corncob although with smallest particle sizes. Adsorption processes on the three adsorbents were best described by Langmuir isotherm and explained by pseudo first order kinetics. There were improvements in adsorption capacity by 3.7 and 11 folds in functionalized corncob and nanocellulose respectively. Adsorption of MO was spontaneous on all adsorbents, exothermic and physical on CC and CCNC however it was endothermic and chemical on FCC.

Compliance with ethical standards

Conflict of interest Authors report no conflict of interest.

References

1. Karim Z, Mathew AP, Grahn M, Mouzon J, Oksman K (2014) Nanoporous membranes with cellulose nanocrystals as functional entity in chitosan: removal of dyes from water. Carbohydr Polym 112:668–676

2. Chan CH, Chia CH, Zakaria S, Sajab MS, Chin SX (2015) Cellulose nanofibrils: a rapid adsorbent for the removal of methylene blue. RSC Adv 5:18204–18212

3. Azeez L, Adejumo AL, Lateef A, Adebisi SA, Adetoro RO, Adewuyi S, Tijani KO, Olaoye S (2019) Zero-valent silver nanoparticles attenuate Cd and Pb toxicities on *Moringa oleifera* via immobilization and induction of phytochemicals. Plant Physiol Biochem 139:283–292

4. Pei A, Butchosa N, Berglunda LA, Zhou Q (2013) Surface quaternized cellulose nanofibrils with high water absorbency and adsorption capacity for anionic dyes. Soft Matter 9:2047–2056

5. Jiang F, Hsieh YL (2014) Amphiphilic superabsorbent cellulose nanofibril aerogels. J Mater Chem A 2:6337–6342

6. Batmaz R, Mohammed N, Zaman M, Minhas G, Berry RM, Tam KC (2014) Cellulose nanocrystals as promising adsorbents for the removal of cationic dyes. Cellulose 21(3):1655–1665

7. Mahfoudhi N, Boufi S (2017) Nanocellulose as a novel nanostructured adsorbent for environmental remediation: a review. Cellulose. https://doi.org/10.1007/s10570-017-1194-0

8. Azeez L, Lateef A, Adebisi SA, Oyedeji AO (2018) Novel biosynthesized silver nanoparticles from cobweb as adsorbent for Rhodamine B: equilibrium isotherm, Kinetic and Thermodynamic studies. Appl Water Sci 8:32. https://doi.org/10.1007/s13201-018-0676-z

9. Wang J, Liu X, Jin T, He H, Liu L (2019) Preparation of nanocellulose and its potential in reinforced composites: a review. J Biomater Sci Polym 30(11):919–946

10. Theivasanthi T, Christma FLA, Adeleke JT, Subash CBG, Ravichandran R (2018) Synthesis and characterization of cotton fiber-based nanocellulose. Int J Biol Macromol 109:832–836

11. Yang X, Han F, Xu C, Jiang S, Huang L, Liu L, Xi Z (2017) Effects of preparation methods on the morphology and properties of nanocellulose (NC) extracted from corn husk. Ind Crops Prod 109:241–247

12. Zhu HY, Jiang R, Fu YQ, Jiang JH, Xiao L (2011) Preparation, characterization and dye adsorption properties of γFe$_2$O$_3$/SiO$_2$/chitosan composite. Appl Surf Sci 258:1337–1344

13. Li X, Xiao W, He G, Zheng W, Yu N, Tan M (2012) Pore size and surface area control of MgO nanostructures using a surfactant-templated hydrothermal process: high adsorption capability to azo dyes. Colloids Surf A 408:79–86

14. Kou T, Wang Y, Zhang C, Sun J, Zhang Z (2013) Adsorption behaviour of methyl orange onto nanoporous core–shell Cu@Cu$_2$O nanocomposite. Chem Eng J 223:76–83

15. Samiey B, Farhadi S (2013) Kinetics and thermodynamics of adsorption of fuchsin acid on nickel oxide nanoparticles. Acta Chim Slov 60:763–773

16. Satapathy MK, Banerjee P, Das P (2013) Plant-mediated synthesis of silver-nanocomposite as novel effective azo dye adsorbent. Appl Nanosci 5:1–9

17. Hsiao Y-C, Wu T-F, Wang Y-S, Hu C-C, Huang C (2014) Evaluating the sensitizing effect on the photocatalytic decoloration of dyes using anatase-TiO$_2$. Appl Catal B 148–149:250–257

18. Mahmoud HR, Ibrahim SM, El-Molla SA (2015) Textile dye removal from aqueous solutions using cheap MgO nanomaterials: adsorption kinetics, isotherm studies and thermodynamics. Adv Powder Technol 1:223–231

19. Istratie R, Stoia M, Pacurariu C, Locovei C (2016) Single and simultaneous adsorption of methyl orange and phenol onto magnetic iron oxide/carbon nanocomposites. Arab J Chem. https://doi.org/10.1016/j.arabjc.2015.12.012

20. Keyhanian F, Shariati S, Faraji M, Hesabi M (2016) Magnetite nanoparticles with surface modification for removal of methyl violet from aqueous solutions. Arab J Chem 9:S348–S354

21. Kumar PS, Varjani SJ, Suganya S (2018) Treatment of dye wastewater using an ultrasonic aided nanoparticle stacked activated carbon: kinetic and isotherm modelling. Bioresour Technol 250:716–722

22. Maiti S, Jayaramudu J, Das K, Reddy SM, Sadiku R, Ray SS, Liu D (2013) Preparation and characterization of nano-cellulose with new shape from different precursor. Carbohydr Polym 98:562–567

23. Chen W, Li Q, Cao J, Liu Y, Li J, Zhang J, Luo S, Yu H (2015) Revealing the structuresof cellulose nanofiber bundles obtained by mechanical nanofibrillation via TEM observation. Carbohydr Polym 117:950–956

24. Deepa B, Abraham E, Cordeiro N, Mozetic M, Mathew AP, Oksman K, Faria M, Thomas S, Pothan LA (2015) Utilization of various lignocellulosic biomass for the production of nanocellulose: a comparative study? Cellulose 22(2):1075–1090

25. Suman S, Kardam A, Gera M, Jain VK (2015) A novel reusable nanocomposite for complete removal of dyes, heavy metals and microbial load from water based on nanocellulose and silver nano-embedded pebbles. Environ Technol 36(5–6):707–714

26. Gautam D, Kumari S, Ram B, Chauhan GS, Chauhan K (2018) A new hemicellulose-based adsorbent for malachite green. J Environ Chem Eng 6(4):3889–3897

27. Liu C, Li B, Du H, Lv D, Zhang Y, Yu G, Mu X, Peng H (2016) Properties of nanocellulose isolated from corncob residue using sulfuric acid, formic acid, oxidative and mechanical methods. Carbohydr Polym 151:716–724

28. Anjum H, Murugesan T (2016) Effect of functionalization condition on characterization of carbonaceous adsorbent. Procedia Eng 148:1346–1350

29. Ojedokun AT, Bello OS (2017) Liquid phase adsorption of Congo red dye on functionalized corncobs. J Dispers Sci Technol 38(9):1285–1294

30. Ojo TA, Ojedokun AT, Bello OS (2017) Functionalization of powdered walnut shell with orthophosphoric acid for Congo red dye removal. Part Sci Technol 37(1):74–85

31. Xu J, Chena L, Qu H, Jiao Y, Xie J, Xing G (2014) Preparation and characterization of activated carbon from reedy grass leaves by chemical activation with H_3PO_4. Appl Surf Sci 320:674–680

32. Yorgun S, Yıldız D (2015) Preparation and characterization of activated carbons from Paulownia wood by chemical activation with H_3PO_4. J Taiwan Inst Chem Eng 53:122–131

33. Duan X, Srinivasakannan C, Wang X, Wang F, Liu X (2017) Synthesis of activated carbon fibers from cotton by microwave induced H_3PO_4 activation. J Taiwan Inst Chem Eng 70:374–381

34. Kumar A, Jena HM (2016) Preparation and characterization of high surface area activated carbon from Fox nut (Euryale ferox) shell by chemical activation with H_3PO_4. Res Phys 6:651–658

35. Shamsuddin MS, Yusoff NRN, Sulaiman MA (2016) Synthesis and characterization of activated carbon produced from kenaf core fiber using H_3PO_4 activation. Procedia Chem 19:558–565

36. Yakout SM, Sharaf El-Deen G (2016) Characterization of activated carbon prepared by phosphoric acid activation of olive stones. Arab J Chem 9:S1155–S1162

37. Macías-García A, Carrasco-Amador JP, Encinas-Sánchez V, Díaz-Díeza MA, Torrejón-Martín D (2019) Preparation of activated carbon from kenaf by activation with H_3PO_4. Kinetic study of the adsorption/electroadsorption using a system of supports designed in 3D, for environmental applications. J Environ Chem Eng 7:103196

38. Saravanan A, Kumar PS, Yaashikaa PR, Kanmani S, Varthine RH, Muthu CMM, Yuvaraj D (2019) Modelling on the removal of dye from industrial wastewater using surface improved Enteromorpha intestinalis. Int J Environ Res 13(2):1–18

39. Huang R, Liu Q, Huo J, Yang B (2017) Adsorption of methyl orange onto protonated crosslinked chitosan. Arab J Chem 10:24–32

40. Rattanapa S, Srikram J, Kongsune P (2017) Adsorption of methyl orange on coffee grounds activated carbon. Energy Procedia 138:949–954

41. Renita AA, Kumar PS, Jabasingh SA (2019) Redemption of acid fuchsin dye from wastewater using de-oiled biomass: kinetics and isotherm analysis. Bioresour Technol Rep 7:100300

42. Tharaneedhar V, Kumar PS, Saravanan A, Ravikumar C, Jaikumar V (2016) Prediction and interpretation of adsorption parameters for the sequestration of methylene blue dye from aqueous solution using microwave assisted corncob activated carbon. Sustain Mater Technol. https://doi.org/10.1016/j.susmat.2016.11.001

43. Langmuir I (1918) The adsorption of gases on plane surfaces of glass, mica and platinum. ACS 40:1361–1403

44. Freundlich HMF (1906) Over the adsorption in solution. J Phys Chem 57:385–470

45. Tempkin MI, Pyzhev V (1940) Kinetics of ammonia synthesis on promoted iron catalyst. Acta Phys Chim USSR 12:327–356

46. Dubinin MM, Radushkevich LV (1947) The equation of the characteristic curve of the activated charcoal. Proc Acad Sci USSR Phys Chem Sect 55:331–337

47. Adekola FA, Ayodele SB, Inyinbor AA (2019) Efficient Rhodamine B removal using acid- and alkaline-activated Musa paradisiaca biochar. Pol J Environ Stud 28(5):3063–3070

48. Hussain S, Anjali KP, Hassan ST, Dwivedi PB (2018) Waste tea as a novel adsorbent: a review. Appl Water Sci 8:165. https://doi.org/10.1007/s13201-018-0824-5

49. Munagapati VS, Wen J-C, Pan C-L, Gutha Y, Wen J-H (2019) Enhanced adsorption performance of Reactive Red 120 azo dye from aqueous solution using quaternary amine modified orange peel powder. J Mol Liq 285:375–385

50. Oyelude EO, Awudza JAM, Twumasi SK (2018) Removal of malachite green from aqueous solution using pulverized teak leaf litter: equilibrium, kinetic and thermodynamic studies. Chem Central J 12:81. https://doi.org/10.1186/s13065-018-0448-8

51. Azeez L, Lateef A, Adejumo AL, Adeleke TA, Adetoro RO, Mustapha Z (2019) Adsorption behaviour of Rhodamine B on hen feather and corn starch functionalized with green synthesized silver nanoparticles (AgNPs) mediated with cocoa pod extracts. Chem Afr. https://doi.org/10.1007/s42250-019-00113-7

52. Abdelwahab O, Amin NK (2013) Adsorption of phenol from aqueous solutions by Luffa cylindrica fibers: kinetics, isotherm and thermodynamic studies. Egypt J Aquat Res 39:215–223

53. Inyinbor AA, Adekola FA, Olatunji GA (2017) Kinetics and isothermal modelling of liquid phase adsorption of Rhodamine B onto urea modified Raphia hookerie epicarp. Appl Water Sci 7(6):3257–3266

54. Inyinbor AA, Adekola FA, Olatunji GA (2017) Liquid phase adsorptions of Rhodamine B dye onto raw and chitosan supported mesoporous adsorbents: isotherms and kinetics studies. Appl Water Sci 7(5):2297–2307

55. He X, Male KB, Nesterenko PN, Brabazon D, Paull B, Luong JHT (2013) Adsorption and desorption of methylene blue on porous carbon monoliths and nanocrystalline cellulose. ACS Appl Mater Interfaces 5:8796–8804

56. Willie C, Hosseini S, Moonis AK, Chuah TG, Thomas SYC (2013) Acid modified carbon coated monolith for methyl orange adsorption. Chem Eng J 215–216:747–754

57. Suganya S, Kumar PS, Saravanan A, Rajan PS, Ravikumar C (2017) Computation of adsorption parameters for the removal of dye from wastewater by microwave assisted sawdust: theoretical and experimental analysis. Environ Toxicol Pharmacol 50:45–57

58. Olajire AA, Abidemi JJ, Lateef A, Benson NU (2017) Adsorptive desulphurization of model oil by Ag nanoparticles-modified activated carbon prepared from brewer's spent grains. J Environ Chem Eng 5:147–159

59. Sahbaz DA, Dandil S, Acikgoz C (2019) Removal of crystal violet dye by a novel adsorbent derived from waste active sludge used in wastewater treatment. Water Qual Res J. https://doi.org/10.2166/wqrj.2019.049

60. Zhou Y, Zhang F, Tang L, Zhang J, Zeng G, Luo L, Liu Y, Wang P, Peng B, Liu X (2017) Simultaneous removal of atrazine and copper using polyacrylic acid functionalized magnetic ordered mesoporous carbon from water. Adsorpt Mech Sci Rep 7:43831. https://doi.org/10.1038/srep43831